

# Synthesis and characterisation of metallic nanoparticles

Nguyen Hoang Luong<sup>1,\*</sup>, Nguyen Ngoc Long<sup>1</sup>, Le Van Vu<sup>1</sup>, Nguyen Hoang Hai<sup>1</sup>,  
Luu Manh Quynh<sup>1</sup>, Phan Tuan Nghia<sup>2</sup>, Nguyen Thi Van Anh<sup>2</sup>

<sup>1</sup>*Center for Materials Science, Hanoi University of Science, Vietnam National University, Hanoi  
334 Nguyen Trai, Thanh Xuan, Hanoi, Vietnam*

<sup>2</sup>*Key Laboratory for Enzyme and Protein Technology, Hanoi University of Science,  
Vietnam National University, Hanoi, 334 Nguyen Trai, Thanh Xuan, Hanoi, Vietnam*

Received 2 December 2009

**Abstract.** Sphere-like gold nanoparticles have been prepared by chemical reduction method and by using X-ray irradiation, while rod-like gold nanoparticles were synthesized according to the seed-mediated growth method and by sonoelectrochemistry. Sphere-like gold nanoparticles have diameter of 20 - 60 nm, while rod-like gold nanoparticles have aspect ratio from 2 to 4. In UV-vis spectra the absorption bands related to surface plasmon resonance were observed. CoPt nanoparticles with the size of 5 - 20 nm have been prepared by electrodeposition, while FePt nanoparticles with the size of 5 - 10 nm were synthesized by sonoelectrodeposition. After annealing, these magnetic nanoparticles showed a high coercivity. The metallic nanoparticles were functionalized for trial of application in biomedicine.

**Keywords:** Gold nanoparticles, CoPt nanoparticles, FePt nanoparticles, Optical properties, Magnetic properties.

## 1. Introduction

Metallic nanoparticles (NPs) are very attractive because of their size- and shape-dependent properties (see, for instance, [1]). For example, gold nanospheres have a characteristic red colour, but anisotropic gold nanorods have a changed dramatically colour. The colour is due to the collective oscillation of the electrons in the conduction band, known as the surface plasmon oscillation [1,2]. The oscillation frequency is usually in the visible region for gold (and silver) giving rise to the strong surface plasmon resonance absorption. The plasmon resonance absorption has an absorption coefficient orders of magnitude larger than strongly absorbing dyes, leading to increased detection sensitivity. Thus many applications in biomedicine of gold NPs became possible. Magnetic NPs based on transition metals Co, Fe... such as CoPt, FePt... have very high potential application in producing new-generation ultra-high-density magnetic recording media because of their good chemical stability and high magnetocrystalline anisotropy observed in the ordered intermetallic phase with  $L1_0$  structure (see, for instance, [3,4]). These materials will contribute to an effort to design a magnetic medium capable of recording densities beyond 1 Tbits/in<sup>2</sup>. Beside, these materials have potential applications in permanent magnetic nanocomposites and biomedicine.

\*Corresponding author. Tel: (84-4) 38584287, E-mail: luongnh@vnu.edu.vn

In this paper, we report on synthesis and characterization of gold NPs as well as CoPt and FePt NPs.

## 2. Experimental

Synthesis of gold nanospheres using chemical reduction method was carried out as follows: 50 ml of 0.01 wt% chlorauric acid ( $\text{HAuCl}_4 \cdot 3\text{H}_2\text{O}$ ) solution was heated to boiling while stirring in a 100 ml beaker. Then a few hundred microlitres ( $\mu\text{l}$ ) of 1 wt% trisodium citrate dihydrate ( $\text{Na}_3\text{C}_6\text{H}_5\text{O}_7 \cdot 2\text{H}_2\text{O}$ ) solution was quickly added to the auric solution. The solution changed colour within several minutes from yellow to black and then to red or purple colour depending on the size of the nanoparticles. Gold nanospheres were also synthesized using a stronger reductive agent (sodium borohydride ( $\text{NaBH}_4$ )) as follows: 5 ml  $\text{NaBH}_4$  0.01 M at 0 °C was added to 25 ml  $\text{HAuCl}_4$  1 mM in 50 ml flask with stirring for 15 min, until the colour of the solution changed from lightly yellow to dark red.

Gold NPs were also synthesized via a photochemical approach by using X-ray irradiation. A few  $\mu\text{l}$  of 1 mM triton X-100 (TX-100) solution was mixed with 3 ml of 1 mM  $\text{HAuCl}_4 \cdot 3\text{H}_2\text{O}$  solution. Pure  $\text{HAuCl}_4$  solution without TX-100 addition was also prepared for comparison. The X-ray radiation was Cu-K $\alpha$  radiation of an X-ray diffractometer Bruker D5005 with the parameters of 40 kV and 40 mA. The X-ray irradiation time was set up to 40 or 60 min to guarantee the complete reduction of gold precursor solution.

Gold nanorods have been synthesized according to the seed-mediated growth method consisting of two steps.

Step 1: Preparation of seed solution: 2.5 ml of 1 mM chlorauric acid solution was mixed with 7.5 mL of 0.2 M cetyltrimetylammonium bromide (CTAB:  $\text{C}_{19}\text{H}_{42}\text{BrN}$ ) solution and stirred. 0.6 mL of ice-cold 0.01 M sodium borohydride ( $\text{NaBH}_4$ ) solution was added to the stirred solution. The final solution had a brownish yellow colour. After stirring the seed solution for 2 min, the seed solution was kept at room temperature (RT).

Step 2: Growth of nanorods: 5 ml of 0.2 M CTAB solution was added to 5 ml of 1 mM chlorauric acid solution. Then a few hundred  $\mu\text{l}$  of 4 mM silver acetate ( $\text{AgC}_2\text{H}_3\text{O}_2$ ) solution was added and gently mixed. After that, to this solution, 70  $\mu\text{l}$  of 0.08 M ascorbic acid ( $\text{C}_6\text{H}_8\text{O}_6$ ) solution and 12  $\mu\text{l}$  of the seed solution were added. By changing the amount of silver acetate, the aspect ratio (AR) defined as the length of the major axis divided by the width of the minor axis of the nanorods can be varied. To separate nanorods from nanospheres, the solution was centrifuged at 3000 rpm for 10 min.

Gold nanorods were also synthesized from metallic gold by sonoelectrochemical technique. A gold metal plate (1 cm  $\times$  1 cm  $\times$  0.05 cm) was used as the anode and a platinum plate (1 cm  $\times$  1 cm  $\times$  0.05 cm) was used as the cathode. These two electrodes were placed in a glass containing 25 ml of electrolytic solution consisted of 0.08 M CTAB and 83 mg tetradodecylammonium-bromide (TCAB). 2 ml of acetone and 1 mL of cyclohexan were added into the above mixed solution prior to electrolysis. Then the glass with the electrolytic solution was putted to an ultrasonic bath (ULTRASONIC LC 30H) and ultrasonicated throughout the electrolysis time.

CoPt NPs were synthesized by electrodeposition method. The electrolytes were composed of 0.1 M/l  $\text{CoCl}_2 \cdot 6\text{H}_2\text{O}$ , 0.01 M/l  $\text{H}_2\text{PtCl}_6$ , and 0.525 M/l  $\text{Na}_2\text{SO}_4$ , contained in a 100 ml three-neck flash. The pH of 3 of the electrolyte was adjusted by  $\text{H}_2\text{SO}_4$ . Poly(vinyl-pyrrolidone) (PVP) with molecule weight of 30,000 as a surfactant was added. Before starting electrodeposition, nitrogen gas was bubbled in the electrolyte for 20 min to remove the amount of dissolved oxygen. Electrodeposition has

been conducted galvanostatically in a two electrode home-made cell at RT. A platinum plate with a square of  $1\text{ cm}^2$  was used as a counter electrode. A titanium cathode has the same area. Current pulse  $J$  was changed from 13 to  $40\text{ mA/cm}^2$ . The duration of the current pulse was 0.5 s then the current was turned off for a fixed duration of 0.3 s. The electrodeposition was carried out under nitrogen atmosphere. After 1 h deposition, a black solution was obtained and as-prepared nanoparticle powder was collected by using centrifuging at 9000 rpm for 30 min. The powder was annealed at  $700^\circ\text{C}$  for 1 h under a mixture of 5 %  $\text{H}_2$  and 95 % Ar atmosphere. The increasing rate of temperature was  $6^\circ\text{C/min}$  and cooling with the furnace.

The sonoelectrodeposition method has been used for synthesis of FePt NPs. The sonoelectrodeposition device employed is similar to that described in ref. [5]. A titanium horn with diameter of 1.3 cm acted as both the cathode and ultrasound emitter (Sonics VCX 750). The electroactive part of the sonoelectrode was the planar circular surface at the bottom of the Ti horn. This sonoelectrode produced a sonic pulse that immediately followed a current pulse. A platinum plate with a square of  $1\text{ cm}^2$  was used as a counter electrode. The current pulse was changed from 15 to  $30\text{ mA/cm}^2$ . The ultrasound power density was  $100\text{ W/cm}^2$ . The duration  $t_{\text{on}}$  of the current pulse was 0.5 s then the current was turned off for a fixed duration of 0.5 s. During  $t_{\text{on}}$ , FePt NPs were deposited on the surface of the electrode. When the current was switched off, an ultrasound was activated to remove the NPs from the electrode. The time of ultrasound was 0.2 s for all samples. The temperature during the reaction was room temperature. After deposition, FePt NPs were collected by using a centrifuge (Hettich Universal 320) at 9000 rpm for 20 min. NPs were dried in air at  $80^\circ\text{C}$  for 20 min. All samples were annealed at  $700^\circ\text{C}$  for 1 h under  $\text{H}_2$  atmosphere.

The obtained NPs were characterized by X-ray diffraction (XRD) by using a Bruker D5005 diffractometer and transmission electron microscopy (TEM) by using a JEOL JEM1010 electron microscope. UV-vis absorption spectra of the nanoparticle solutions were collected with a Shimadzu UV 2450 PC spectrometer. The chemical composition of the CoPt and FePt NPs was studied by using an energy dispersion spectroscopy (EDS OXFORD-ISIS 300). Magnetic measurements were performed by using a DMS-880 sample vibrating magnetometer (VSM) with maximum magnetic field of 13.5 kOe at RT.

### 3. Results and discussion

#### *Gold nanoparticles*

Figure 1 shows a typical XRD pattern of the gold NPs obtained from the solution with  $400\ \mu\text{l}$  of trisodium citrate solution. It can be seen from the figure that all the diffraction peaks corresponding to the diffraction planes (111), (200) and (220) were indexed to the gold metal with face-centered cubic (fcc) structure. Lattice constant determined from XRD pattern is  $a = 4.078\ \text{\AA}$ , in good agreement with the standard diffraction pattern of cubic gold metal (Pattern 4-784) [6].

Surface plasmon absorption spectra of spherical gold NPs prepared with different amounts of 1 % trisodium citrate solution are shown in figure 2. As seen from the figure, the maximum of the absorption spectrum is shifted to the short wavelength side (from  $539.9\text{ nm}$  to  $521.1\text{ nm}$ ) and the full width at half maximum (FWHM) of the spectrum is decreased with increasing amount of trisodium citrate from  $200\ \mu\text{l}$  to  $400\ \mu\text{l}$ . Thus, the amount of citrate solution determines the size of the NPs. The faster the capping of the NPs by the citrate, the smaller the resulting NPs.

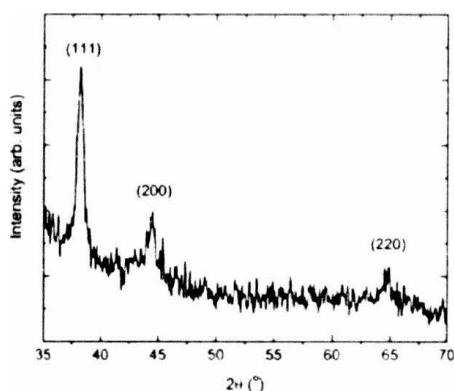


Fig. 1. XRD pattern of the gold NPs prepared by chemical reduction technique.

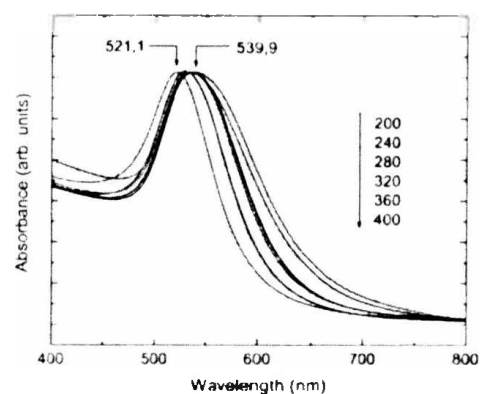


Fig. 2. Surface plasmon absorption spectra of spherical gold NPs prepared with different amounts of 1% trisodium citrate solution: 200, 240, 280, 320, 360 and 400  $\mu$ l.

Typical TEM images of the gold NPs prepared with different amounts of 1% trisodium citrate solution are shown in figure 3. From the figure one can see that when the amount of trisodium citrate increases from 200  $\mu$ l to 400  $\mu$ l, the size of the synthesized gold NPs decreases from 60 nm to 30 nm. That means the more amount of trisodium citrate, the smaller obtained NPs.

Gold NPs were also synthesized via a photochemical approach by using X-ray irradiation as mentioned above. The TEM image [6] showed that the addition of TX-100 behaving as a particle stabilizer and reducing agent into  $\text{HAuCl}_4$  solution tremendously affected the formation and growth of the gold NPs.

Gold nanorods were synthesized according to the seed-mediated growth method with two steps. TEM image of gold NPs for the as-prepared sample (not shown) showed that two major components of the sample are spherical NPs and nanorods. After centrifugation at 3000 rpm for 10 min, the nanorods were separated from spherical NPs.

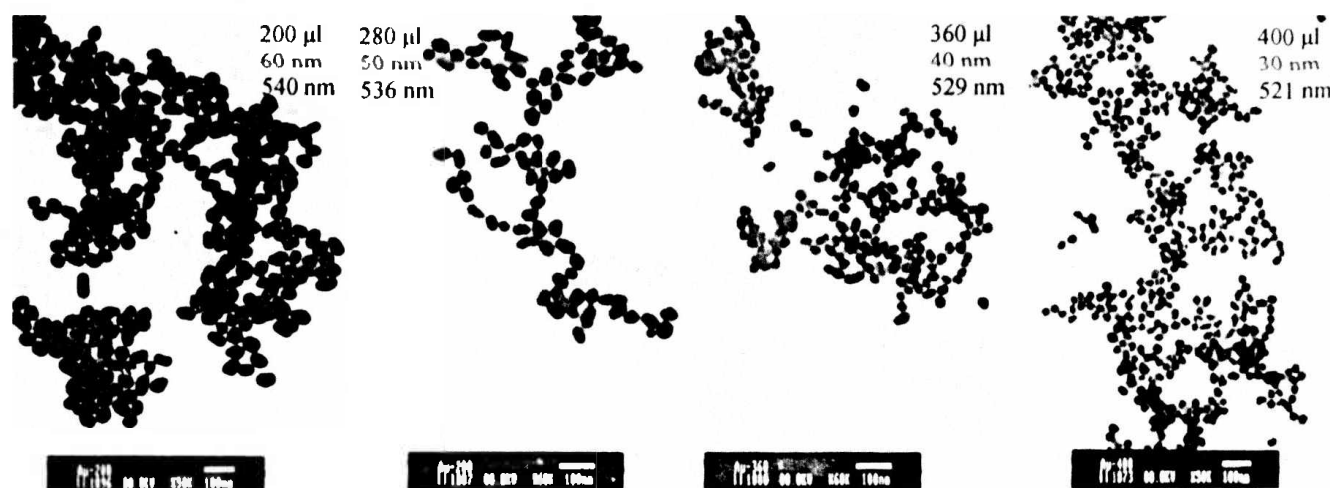


Fig. 3. TEM images of the gold NPs prepared with different amounts (200, 280, 360 and 400  $\mu$ l) of 1% trisodium citrate solution. All the scale bars are 100 nm. On the pictures are shown the size of the NPs and the wavelength of the maximum of surface plasmon absorption spectra.

Surface plasmon absorption spectra of anisotropic gold nanorods prepared with different amounts of 4 mM silver acetate solution are shown in figure 4. As seen from the figure, when the shape of the NPs changes from nanospheres to nanorods, the surface plasmon absorption spectra also change. The surface plasmon absorption spectra of the gold nanorods have two bands: one band in the blue-green

region around 525 nm due to the transverse oscillation of electrons and another band in the red-nearinfrared region due to the longitudinal electronic oscillation. In addition, the position of the band due to the transverse electronic oscillation is almost unvaried; meanwhile with increasing the silver acetate content from 70  $\mu\text{l}$  to 120  $\mu\text{l}$ , the position of the band due to the longitudinal oscillation is increased from 654 nm to 830 nm, which corresponds to the enhance of the aspect ratio (AR) of the gold nanorods.

Gold nanorods were synthesized from metallic gold by sonoelectrochemical technique as well [7].

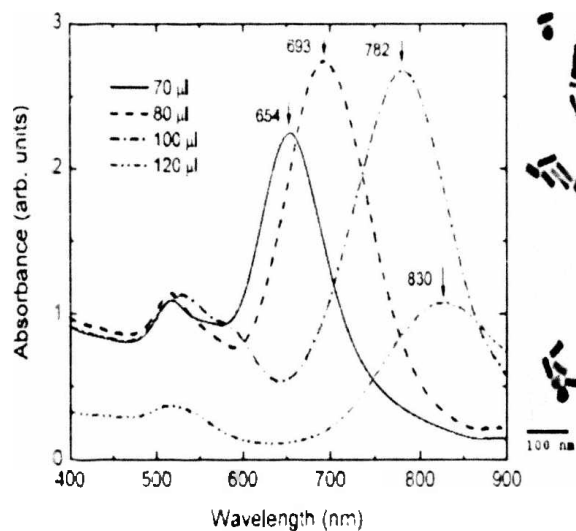


Fig. 4. Surface plasmon absorption spectra of the gold nanorods prepared with different amounts (70, 80, 100 and 120  $\mu\text{l}$ ) of 4 mM silver acetate solution.



Fig. 5. TEM images of the gold nanorods prepared by sonoelectrochemical method. Inset is an aspect ratio distribution histogram.

Typical TEM images of the gold nanorods shown in figure 5 indicate that the nanorods are of uniform size. The AR distribution histogram presented in the inset of figure 5 shows that the size of nanorods has a narrow distribution: the nanorods having the AR of 3 make up 55% and those having the AR of 4 make up 25%.

### CoPt nanoparticles

Before annealing, the XRD patterns for CoPt NPs (not shown) showed the reflections of pure Pt structure, which is similar to other CoPt thin films produced by electrodeposition [8]. The reflections from Co are very weak due to the fact that their atomic weight is much less than that of Pt. The Pt peaks in the as-prepared samples are broad due to the small size of the particles. The as-prepared particles were not disordered CoPt but they were formed by many Co-rich and Pt-rich small particles. Using the Scherrer formula with the FWHM of the strongest peak (111), the mean particle size of the particles was deduced to be 6 nm.

The positive  $\text{Pt}^{4+}$  and  $\text{Co}^{2+}$  ions went to the cathode surface and received electrons to make Pt and Co NPs. If there was not PVP surfactant, Co and Pt atoms would continuously deposited on the particles and at the end we would have a film of CoPt. The presence of PVP around NPs created a steric forces that limit the growth of NPs and we could obtained Co- and Pt NPs well dispersed in the solution.

Figure 6 are the TEM images of typical as-prepared and annealed samples. Particle size of the as-prepared CoPt sample was about 5 nm, which is consistent with the size obtained from the broad XRD peaks. Particle size (5 - 20 nm) depends on the concentration of PVP (1 to 5 g/l). After annealing the particle size increased to 100 nm due to the diffusion and aggregation between particles to form face-centered tetragonal (fct) CoPt NPs.

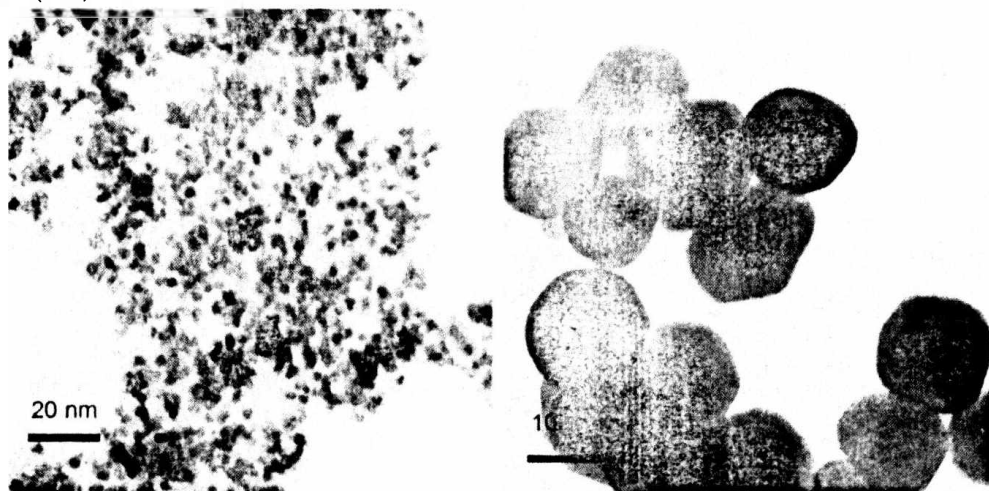


Fig. 6. TEM images of the as-prepared (left) and annealed (right) Co-Pt NPs.

Magnetic measurements revealed low saturation magnetization ( $M_s$ ) and coercivity ( $H_c$ ) in all as-prepared samples (data not shown). The low value of  $M_s$  of the as-prepared NPs may be explained by the oxidation or hydroxidation of Co atoms in NPs which can result in the antiferromagnetic cobalt oxides and weak magnetic cobalt hydroxides. This is in agreement with the suggestion of separated Co and Pt domains in as-prepared NPs. After annealing the hard magnetic CoPt phase was formed. Figure 7 presents the magnetic curves of the annealed samples with current density  $J$  of 13, 20, and 40 mA/cm<sup>2</sup>. The curves for  $J$  of 15, 25, 30 mA/cm<sup>2</sup> (not shown) are similar to that of 20 mA/cm<sup>2</sup>. The curves show typical hard magnetic hysteresis loops of multiphase materials with high  $H_c$ . (For  $H_c$  in the multiphase materials the reader is referred to discussion below for FePt NPs). Coercivity gets maximum value (around 11 kOe) in the samples with the chemical composition of the particles close to the equiatomic composition, i.e., samples with  $J$  of 15 to 30 mA/cm<sup>2</sup>. The atomic percent of Co increased with  $J$  which resulted in the high  $M_s$ . However, the magnetic squareness  $M_r/M_s$  reduced with  $J$  because of the presence of the Co<sub>3</sub>Pt.

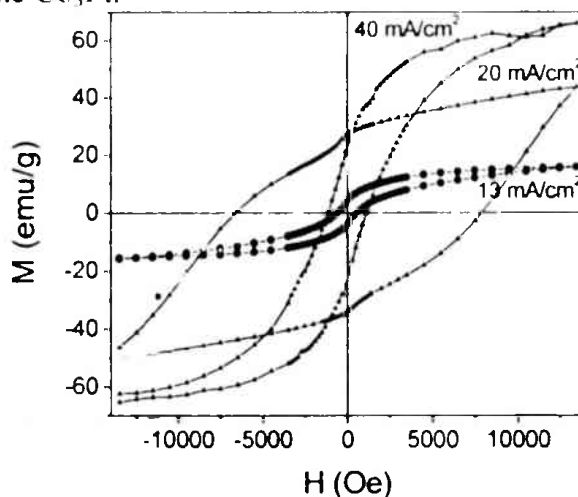


Fig. 7. Magnetic curves for the annealed CoPt samples with  $J$  of 13, 20, and 40 mA/cm<sup>2</sup>.

### FePt nanoparticles

The chemical composition of the FePt NPs was controlled by adjusting the current density (corresponding to the applied voltage). With the current density  $J$  of 15 - 20 mA/cm<sup>2</sup>, the composition of NPs was close to the expected equiatomic composition, namely for  $J$  of 15 mA/cm<sup>2</sup> and 20 mA/cm<sup>2</sup>, Fe<sub>45</sub>Pt<sub>55</sub> and Fe<sub>52</sub>Pt<sub>48</sub> NPs were obtained, respectively. At higher current densities, the atomic percent of Fe was higher because the standard electrode potential Fe<sup>2+</sup>/Fe (-0.44 V [9]) is more negative than that of Pt<sup>4+</sup>/Pt (0.742 V [10]).

As in the case of CoPt NPs, before annealing, the XRD results (not shown) showed the reflections of pure Pt structure, which is similar to other FePt thin films produced by electrodeposition [11]. Upon annealing, the formation of the ordered L1<sub>0</sub> fct phase happened by the diffusion process between Fe and Pt domains. The TEM images of typical as-prepared and annealed samples [12] showed that particle size of the as-prepared FePt sample was 5 - 10 nm, compared to 5.2 nm obtained from the XRD results by using the Scherrer formula. After annealing the particle size increased to 10 - 25 nm due to the aggregation and particle growth.

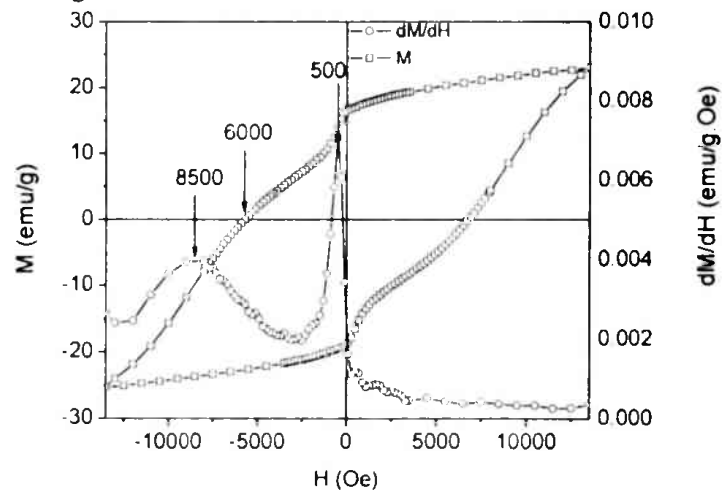


Fig. 8. Magnetic curves of Fe<sub>45</sub>Pt<sub>55</sub> NPs. The maximum applied field is 13.5 kOe.

Magnetic measurements revealed low  $M_s$  and  $H_c$  in all as-prepared samples (data not shown). For the unannealed particles  $M_s$  is about few emu/g and the coercivity is 20 - 80 Oe. The low value of  $M_s$  of the as-prepared NPs may be explained by the oxidation or hydroxidation of Fe atoms in NPs which can result in the weak magnetic iron oxides and iron hydroxides. This is in agreement with the suggestion of separated Fe and Pt domains in as-prepared NPs.

After annealing the hard magnetic FePt phase was formed. Figure 8 presents the magnetic curve of the annealed Fe<sub>45</sub>Pt<sub>55</sub> NPs as an example. The curve shows a typical hard magnetic hysteresis loops with high  $H_c$ . Note that, because of the limit of maximum applied field of 13.5 kOe, the curve is a minor loop. Therefore, the real coercivity must be higher than those obtained from the hysteresis curves. The loop shows a kink at low reversed magnetic field of 500 Oe, which indicates that there was a small amount of a soft magnetic phase. Classically, the coercivity is defined as the field for which the magnetization ( $M$ ) vanishes ( $H'_c$ ). In a more physically meaningful definition, the coercivity  $H_c$  may be defined as the field where the largest number of moments reverses, i.e., the maximum of the susceptibility ( $dM/dH$ ). In most cases, both definitions of the coercivity are almost equivalent. However in multiphase materials, two definitions are significantly different [13]. From Fig. 8,  $H'_c$  was 6 kOe whereas  $H_c$  was 8.5 kOe. Magnetic measurements for all samples show that the atomic percent

of Fe increased with  $J$  which resulted in the high  $M_s$ . However, the magnetic squareness  $M_r/M_s$  reduced with  $J$  because of the presence of the  $\text{Fe}_3\text{Pt}$ .

### ***Application of gold nanoparticles for detecting breast cancer cells***

In order to detect breast cancer cells, we have conjugated the sodium borohydride (or sodium citrate) reduced gold NPs with anti-Her2 antibody (trastuzumab) through either non-covalent or covalent linkages. The procedure consists of the following steps [14]:

#### ***Functionalizing gold nanoparticles with 4-ATP ( $\text{C}_6\text{H}_7\text{NS}$ )***

Different volumes of 4-ATP 2 mM were added into 20 ml of the gold NPs containing solution. The colors of the solutions changed from dark red to dark blue, and then were incubated for 2 days.

#### ***Conjugation of trastuzumab to gold nanoparticles***

Trastuzumab was non-covalently conjugated to colloidal gold NPs, prepared by  $\text{NaBH}_4$  reduction (named as  $\text{BH}_4^*\text{GNPs}$ ). The colloidal gold suspension was adjusted by 0.1 M NaOH to pH 6.5 to react with a mixture of 6  $\mu\text{g}/\text{ml}$  non-labeled trastuzumab and FITC-trastuzumab (480 nm / 520 nm) at mole ratio 10:1 at RT for 5 min. The trastuzumab-GNPs was collected by centrifugation at 4°C, at the rate of 30,000 rpm, for 30 min. The pellets were washed twice and then resuspended in PBS with pH 7.4 containing 0.2 % bovine serum albumin (BSA). Trastuzumab was covalently linked to amino-GNPs through EDC connection. Briefly, the above prepared amino-GNPs was reacted with EDC 0.2 mM in MOPS buffer with pH 6.0, for 20 min. at RT. Then, the EDC\*GNPs were reacted with 6  $\mu\text{g}/\text{ml}$  non-labeled trastuzumab and FITC-trastuzumab (480 nm / 520 nm) at mole ratio 10:1, for 30 min. at RT. The trastuzumab-EDC\*GNPs were washed three times by centrifugation at the rate of 13,000 rpm, at 4°C, for 13 min with PBS and then was stocked in PBS with pH 7.4 containing 0.2 % BSA.

The absorbance profile of trastuzumab-GNPs was measured and compared with that of GNPs using Spectrophotometer (Nanodrop).

#### ***Culture of KPL4 and Hela cells***

KPL4 and Hela cells were cultured in 24-well ELISA plates containing DMEM (Difco Modified Eagle Medium) plus 10 % FBS (Fetal Bovine Serum). Glass coverslips were added in each well and the cells were incubated at 37°C, 5 %  $\text{CO}_2$  to reach a population of about  $4 \times 10^5$  to  $10^6$  cells/ml. The coverslips were picked out to new 24-well ELISA plate for further immuno-nanogold incubation.

#### ***Incubation of trastuzumab- conjugated gold NPs with KPL4, Hela cells and imaging of the cells***

Coverslips containing KPL4 and Hela cells were washed 3 times with 500  $\mu\text{l}$  PBS before being fixed by 3 % paraformaldehyde at RT, for 15 min. and then treated with 5 % triton X-100 at RT for 5 min. After being blocked with 500  $\mu\text{l}$  of 2 % BSA, the coverslips were incubated with 200  $\mu\text{l}$  either of trastuzumab- $\text{BH}_4^*\text{GNPs}$  or trastuzumab-EDC\*GNPs at a concentration of 3  $\mu\text{g}/\text{ml}$  at RT, for 60 min. The coverslips were observed under Axio Plan epifluorescence microscope (Carl Zeiss). The KPL4 cell incubated with Trastuzumab-EDC\*GNPs were observed under FESEM (Field Emission Scanning Electron Microscope).

We could observe the 10 times higher fluorescent intensity of FITC on KPL4 cells than that of FITC on Hela cells in all the three types of trastuzumab-conjugated gold NPs. Because KPL4 is the cell line having a high level of Her2-expression, while Hela is the cell line, which expresses Her2 normally, the remarkable difference in the fluorescent intensity between KPL4 and Hela indicates the specific binding of all the three types of trastuzumab-GNPs on KPL4 membranes. However, among the three types of the trastuzumab-conjugated gold NPs, the covalently linked trastuzumab-EDC\*GNPs showed to be the most stable in fluorescent intensity after a long time of stocking (several months).

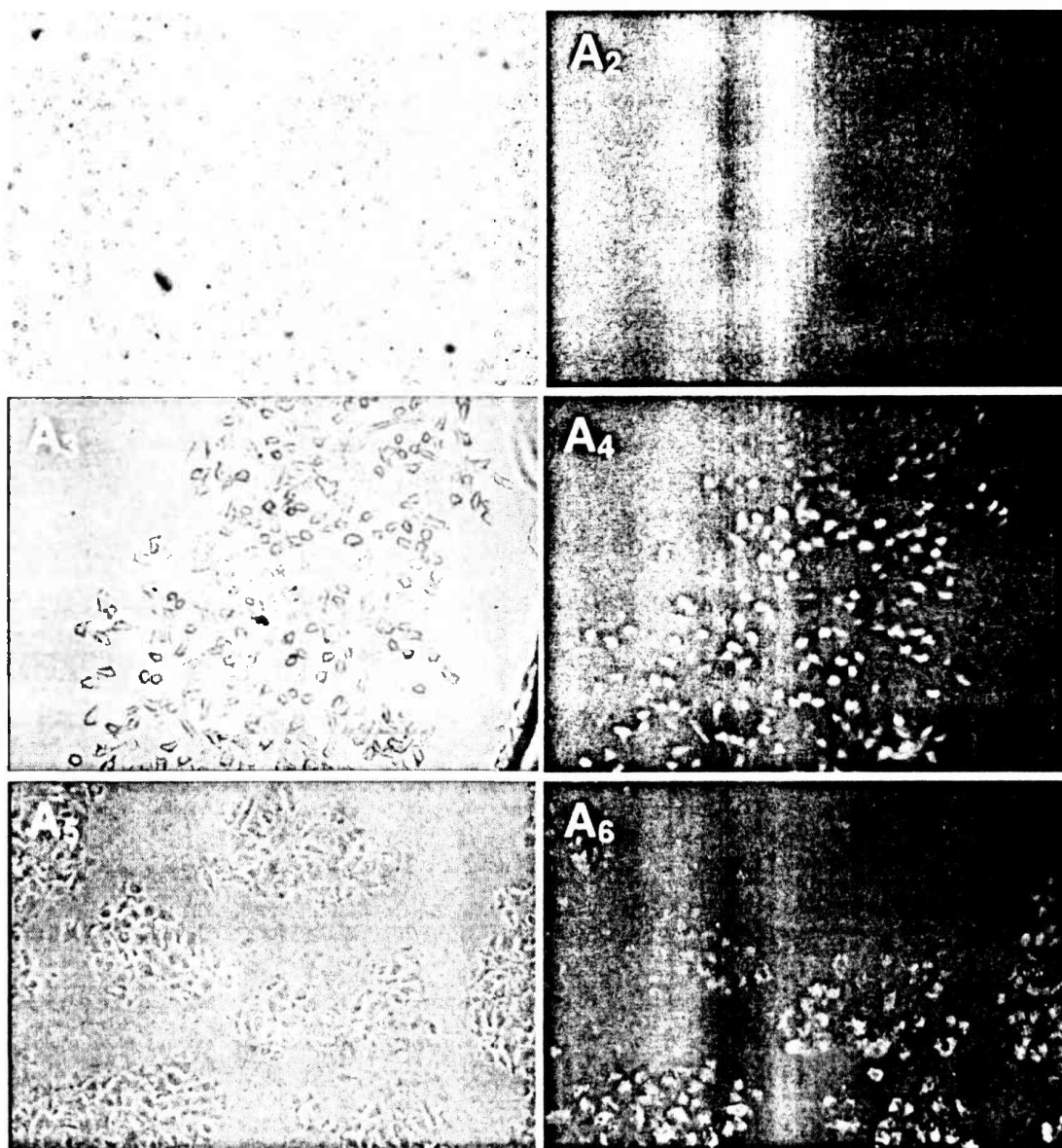


Fig. 9. Typical bright-field ( $A_1$ ,  $A_3$ ,  $A_5$ ) and dark-field ( $A_2$ ,  $A_4$ ,  $A_6$ ) microscopy images of breast cancer cells after incubation with the gold NPs non-conjugated with trastuzumab ( $A_1$ - $A_2$ ), the gold NPs conjugated with trastuzumab ( $A_3$ - $A_4$ ) and the amino-GNPs covalently conjugated with trastuzumab through EDC connection ( $A_5$ - $A_6$ ).

We also tried to conjugate the gold NPs with trastuzumab without FITC fluorescent dye. As seen from figure 9, in the case of the GNPs non-conjugated with trastuzumab, the gold NPs could not find the cancer cells and nothing was observed in the dark-field microscopy image ( $A_2$ ). When the gold NPs were directly conjugated with trastuzumab, the gold NPs concentrated on the cancer cells and these cancer cells were clearly observed in the dark-field microscopy image ( $A_4$ ) by means of scattering light of the gold NPs. When the amino-GNPs were covalently conjugated with trastuzumab through EDC connection, the gold NPs concentrated on the cancer cells as well, but these cancer cells were observed with slightly lower intensity in the dark-field microscopy image ( $A_6$ ) in comparison with those in the image  $A_4$ . However, the gold NPs directly conjugated with trastuzumab were storable in freezer for only about two weeks and then lost their activity; while the gold NPs covalently conjugated with trastuzumab were stable for about two month storage.

#### 4. Conclusion

Gold NPs, CoPt and FePt NPs have been prepared. After annealing, CoPt and FePt NPs showed a high coercivity. We succeeded in conjugating Trastuzumab to gold NPs for specific detection of Her2 over-expressed breast cancer cells, here is KPL4 cell line. Among 3 types of conjugation, the covalently linked Trastuzumab-EDC\*GNPs showed long-time stability and strong binding toward breast cancer cell KPL4.

**Acknowledgments.** The authors would like to thank Ministry of Science and Technology of Vietnam (Contract No 38/355/2008/HD-NDT for Task of Protocol with Israel) and Vietnam National University, Hanoi (Key Project QGTD.08.05) for financial support. The authors are grateful to Nguyen Duy Thien, Chu Dinh Kiem, Sai Cong Doanh, Nguyen Dang Phu of Center for Materials Science, Hanoi University of Science, and Tran Thi Thanh Thoa of Key Laboratory for Enzyme and Protein Technology, Hanoi University of Science for assistance.

#### References

- [1] S. Eustis, M. A. El-Sayed, *Chemical Society Review* 35 (2006) 209.
- [2] L. M. Liz-Marzan, *Materialstoday* 7 (2004) 26.
- [3] Y. Huang, H. Okumura, G.C. Hadjipanayis, in: *Magnetic storage systems beyond 2000*, ed. G.C. Hadjipanayis, Kluwer Academic Publisher, 2001, p. 171.
- [4] S. Sun, *Adv. Mater.* 18 (2006) 393.
- [5] J.J. Zhu, S.T. Aruna, Yu. Koltypin, A. Gedanken, *Chem. Mater.* 12 (2000) 143.
- [6] Nguyen Ngoc Long, Le Van Vu, Chu Dinh Kiem, Sai Cong Doanh, Cao Thi Nguyet, Pham Thi Hang, Nguyen Duy Thien, Luu Manh Quynh, *Journal of Physics: Conference Series* 187 (2009) 012026.
- [7] Nguyen Duy Thien, Chu Dinh Kiem, Nguyen Ngoc Long, *The 6th Vietnam National Conference on Solid State Physics and Materials Science (SPMS-2009)*, Da Nang, Vietnam. 8-10 November, 2009.
- [8] L. Zana, G. Zangari, *J. Magn. Magn. Mater.* 272-276 (2004) 1698.
- [9] P. Atkins, *Physical Chemistry*, 6th edition, W.H. Freeman and Company, New York, 1997.
- [10] A.J. Bard, L.R. Faulkner, *Electrochemical Methods. Fundamentals and Applications*, 2nd edition, John Wiley and Sons Inc., 2001.
- [11] Q. Zeng, Y. Zhang, H.L. Wang, V. Papaefthymiou, G.C. Hadjipanayis, *J. Magn. Magn. Mater.* 272-276 (2004) e1223.
- [12] Nguyen Hoang Luong, Nguyen Hoang Hai, Nguyen Dang Phu, *VNU Journal of Science, Mathematics - Physics* 25 (2009) 1.
- [13] D. Givord, M.F. Rossignol, Coercivity, in J.M.D. Coey (Ed.), *Rare-earth Iron Permanent Magnets*, Clarendon Press: Oxford, 1996, p. 218.
- [14] Luu Manh Quynh, Tran Quoc Tuan, Nguyen Ngoc Long, Nguyen Hoang Luong, Nguyen Hoang Hai, Tran Thi Thanh Thoa, Nguyen Thi Van Anh, Phan Tuan Nghia, *The International Workshop on Advanced Materials and Nanotechnology (IWAMN2009)*, Hanoi, Vietnam, 24-25 November, 2009, to be published in e-Journal of Surface Science and Nanotechnology.